



LONG TERM CLOUD COVER AND SST INVESTIGATION OF THE BLACK SEA

*Mehmet Tahir Kavak*¹, Sabri Karadogan², Sedat Karayücel³*

¹Department of Physics, Dicle University, 21280 Diyarbakir, Turkey

²Department of Geography, Dicle University, 21280 Diyarbakir, Turkey

³Department of Aquaculture, Sinop University, 57100, Sinop, Turkey

* mtkavak@dicle.edu.tr

One important of satellite remote sensing is the count of cloudy days of a particular region. Cloud cover hampers radiation received from the sun therefore controls LST (land surface, SST (Sea Surface Temperature) accordingly humidity, evaporation, agriculture, aquaculture, tourism, and other human activities.

Present work investigated long term cloud cover of the Black Sea using high resolution 6927 daily and 207 monthly composite AVHRR satellite data from March 1993 to December 2012. The results could give a clue for regional and global climate change to take an action for the feature. Results mapped potential availability of obtaining cloud free images for use of other disciplines.

The results were discussed as well as the geographical planetary factors that determine the climate of the Black Sea basin and in the context of global climate change. The results obtained also for other disciplines (climate, meteorology, oceanography, hydrography, biology, environmental science, agriculture, tourism, such as Industry) will create a data source. SST patterns also revealed oceanographic events which was studied in earlier work too.

Key words: Black Sea; AVHRR; Cloud cover, SST; Remote Sensing, Global Warming

1. Introduction

The Black Sea is a sea in Southeastern Europe. It is bounded by Europe, Anatolia and the Caucasus, and drains through the Mediterranean into the Atlantic Ocean, via the Aegean Seas and various straits. The Bosphorus Strait connects it to the Sea of Marmara, and the Strait of the Dardanelles connects that

sea to the Aegean Sea region of the Mediterranean. These waters separate Eastern Europe and western Asia. The Black Sea is also connected to the Sea of Azov by the Strait of Kerch.

The Black Sea has an area of 436,400 km² (not including the Sea of Azov) [1], a maximum depth of 2,212 m[2], and a volume of 547,000 km³[3] The Black Sea forms in an east-west trending elliptical depression which lies between Bulgaria, Georgia, Romania, Russia, Turkey, and Ukraine[4]. It is constrained by the Pontic Mountains to the south and by the Caucasus Mountains to the east, and features a wide shelf to the northwest. The longest east-west extent is about 1,175 km.

The Black Sea has a positive water balance; that is, a net outflow of water 300 km³ per year through the Bosphorus and the Dardanelles into the Aegean Sea. Mediterranean water flows into the Black Sea as part of a two-way hydrological exchange. The Black Sea outflow is cooler and less saline, and floats over the warm, more saline Mediterranean inflow – as a result of differences in density caused by differences in salinity – leading to a significant anoxic layer well below the surface waters. The Black Sea also receives river water from large Eurasian fluvial systems to the north of the Sea, of which the Don, Dnieper and Danube are the most significant.

2. Materials and Methods

2.1. Cloud Cover

When the world's first satellite pictures of the atmosphere were viewed, the most striking feature was the extensive cloud cover over large parts of the Earth. Even today, the first feature that is usually noticed in a meso-scale satellite image is the clouds.

Typically 50 percent of the Earth's surface is covered by cloud at any time [5]. Clouds seen on a satellite image are of course of great importance from the meteorological point of view. However, in studying the surface of the Earth, the necessary information in that case can only be obtained if the path of the electromagnetic radiation, which is the carrier of the information between the satellite and the surface of the Earth, is free from any obstacle, which in this case is the cloud field.

Clouds have a severe effect on the infrared and visible radiation that is received by satellite. Clouds have to be removed from the satellite imagery if the Earth's surface is going to be observed using optical remote sensing techniques. For example, the effect of clouds on the average SST received by satellite can be seen in Fig.1.

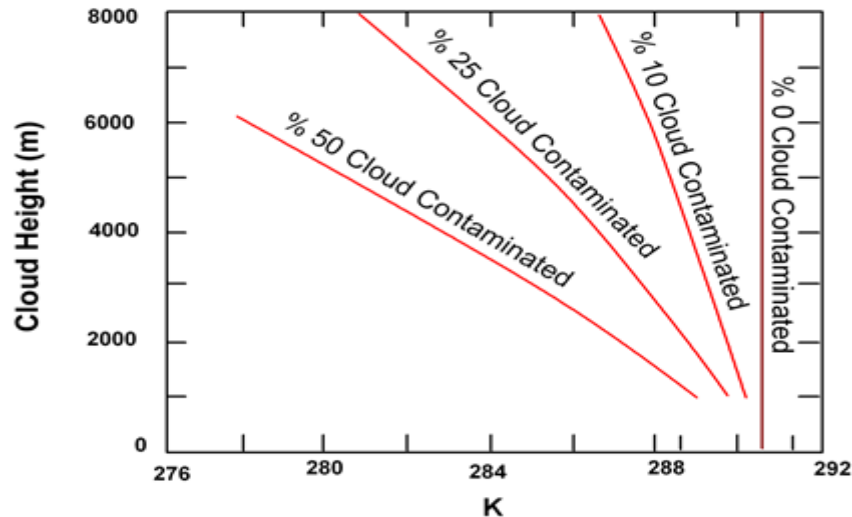


Figure 1. Effect of clouds partially filling the nadir field of view in the 10.5-12.5 μ m region. Calculations are for the VHRR (Maul, 1985).

2.2. Sea Surface Temperature

One of the most useful data sets offered by remote sensing of oceans is SST, SST is defined as the water temperature close to the ocean's surface about 20 m [6]. Thermal IR sensors on environmental satellites can be used to measure the temperature across large expanses of the ocean surface [7]. Satellite data has many important applications, such as ship routing and fisheries (Brown et al., 1993), the detection and monitoring of ocean currents [7-13], water fronts, eddies and rings [14-22], shallow sea fronts [23], upwelling zones [24], sea ice cover [25-27,] ice movement [28,29], polar meteorology [30-33], flood monitoring [34-36] and current vectors [37-40]

SST affects the behavior of the Earth's atmosphere above, so their initialization into atmospheric models is important. While sea surface temperature is important for tropical cyclogenesis, it is also important in determining the formation of sea fog and sea breezes [41]. Heat from underlying warmer waters can significantly modify an air mass over distances as short as 35 kilometers to 40 kilometers [42]. For example, southwest of Northern Hemisphere extra tropical cyclones, curved cyclonic flow bringing cold air across relatively warm water bodies can lead to narrow lake-effect snow (or sea effect) bands. Those bands bring strong localized precipitation, often in the form of snow, since large water bodies such as lakes efficiently store heat that results in significant temperature differences—larger than 13 °C between the water surface and the air above [43,44]. Because of this temperature difference, warmth and moisture are transported upward, condensing into vertically oriented clouds which produce snow showers. The temperature decrease with height and cloud depth are directly affected by both the water temperature and the large-scale environment. The stronger the temperature decrease with height, the taller the clouds get, and the greater the precipitation rate becomes [45,46].

Black Sea was studied as it has a large influence on regional global climate and weather. Seasonal SST field and interannual variability of Black Sea using AVHRR studied from 1982 to 2000 [47], physical oceanography of the Black Sea [48], Circulation in the surface and intermediate layers of the Black Sea [49].

2.3. Study Area



Figure 2. Geographic setting and bathymetry of the Black Sea.

To perform cloud cover and SST investigation of the Black Sea (Fig.2) NOAA-AVHRR HRPT data has been used. HRPT (High Resolution Picture Transmission) data were acquired from the DLR (German Aerospace Center) via the Internet (DLR, 2013) Earth Observation on the WEB interface (EOWEB). Cloud removal process was performed by DLR. AVHRR data was chosen for investigation of cloud cover over the Black Sea for the following reasons as it has Large swath width (3000km) compared to the width (east west), spatial resolution (1km), spectral resolution (4 or 5 AVHRR channels), temporal resolution (a daily SST image from DLR is formed by using up to five acquisitions), availability (data on line), cost (free), and data processed (ready for analysis). A total of 6927 daily composites images were downloaded for processing. According to the DLR each daily image has been acquired from at least five NOAA-AVHRR passes; this gives a total of 34635 passes or more. The numbers of available data sets are listed in table 1.

Table 1. List of 6927 daily composite images acquired from DLR.

	Jan	Feb	Mar	Apr	May	Jun	Jul	Aug	Sep	Oct	Nov	Dec
1993			31	30	31	30	31	31	30	31	29	31
1994	30	28	31	30	31	30	31	31	30	31	30	31
1995	29	28	31	30	31	30	30	31	30	31	30	31
1996	30	29	31	30	31	30	30	31	30	31	30	31
1997	30	26	29	30	30	30	31	30	30	30	29	31
1998	31	27	31	30	29	30	31	31	30	30	30	29
1999	30	28	29	29	29	30	31	29	30	31	30	31
2000	31	29	31	30	31	30	31	31	29	31	30	31
2001	30	28	31	30	31	30	31	31	30	31	30	18
2002				30	31	30	31	31	30	31	30	30
2003	31	28	31	28	31	30	31	31	28	31	30	31
2004	24	29	17	25	31	30	31	29	29	31	29	28
2005	30	28	31	29	30	29	31	31	30	30	30	30
2006	31	28	30	29	31	30	31	31	26	25	24	24
2007	31	27	29	30	31	30	31	31	30	31	30	31
2008	31	28	31	30	31	30	31	31	30	31	30	31
2009	31	28	31	30	30	30	30	18			30	31
2010	31	28	31	30	26	30	31	30	30	31	30	30
2011	31	28	31	29	31	30	31	31	29	31	30	27
2012	17	29	31	29	30	29	31	31	30	28	28	31

2.4. Data Processing

In order to analyze and generate cloud cover patterns for individual months, PIXEL41 software was written in Fortran 90 programming language. First, all the files have to be converted into raw file format; this was achieved by using the Paint Shop Pro [50] image processing software.

The software (PIXEL41) counts the number of cloud (255) pixels in a particular point from multiple images. It reads pixels on each row and records the number of digital values of (representing cloud) 255 into a new binary raw image until it finishes all rows. At the end of the process, an image file is produced that represents cloud density of the input month (see Fig.3).

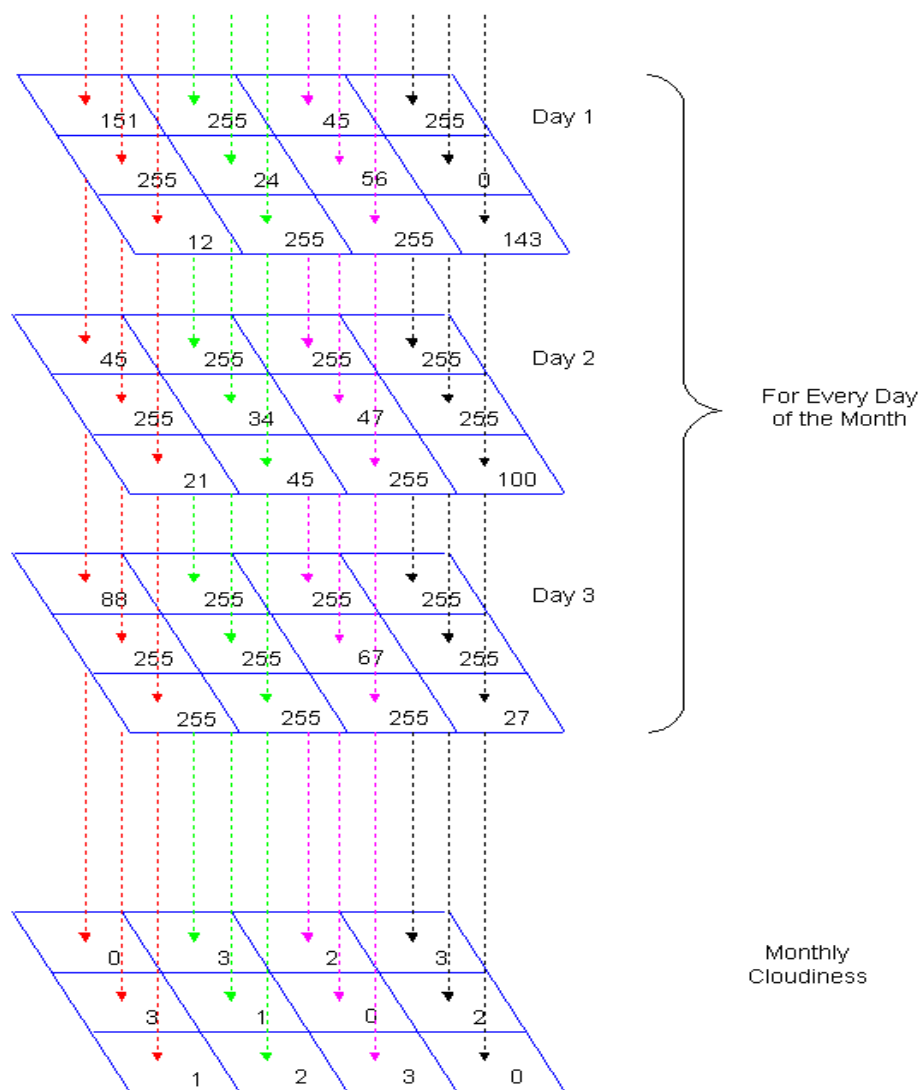


Figure 3. Schematic diagram of how monthly cloudiness is computed from daily input files.

When all the daily files for each month of each year was processed, there were a total of 233 images representing cloud density (This images will not be displayed as it will exceed the length of the paper) of the individual months 20 yearly and 12 monthly over and the twenty year period.

Once the process described above was completed, the 233 monthly files were imported individually to ERMapper to create resized and pseudo colored of all months. The mean monthly mean was calculated from the monthly images results were presented on table 2, table 3 and plotted in Fig.4-5 and generated pattern in Figure 6 and Fig.7.

2.5. Sea Surface Temperature

The monthly MCSST data with the resolution of 1 km AVHRR from March 1993 to December 2012 was downloaded. The SST values are stored as follows: Greyvalue “0” is reserved for “LAND”, greyvalue “255” is reserved for “CLOUD” and no “NO DATA” The temperature range starts with 0.0oC and is referred to greyvalue “1”. The radiometric resolution is 0.125oC; greyvalue 254 is therefore referred to 31.75oC (maximum temperature). Images were containing whole Europe, so to study the area of interest (The Mediterranean Sea) whole images were imported to ERMapper 5.2 (ERMapper). Then the SST of each month for MS was calculated excluding flagged pixels A total of 206 monthly composite SST images were downloaded from aforementioned DLR web site to process SST of the BS. The result presented on Figure 8.

3. Results And Discussions

3.1. Cloud Cover

Table 2. Statistical table of monthly average cloudiness.

	Jan	Feb	Mar	Apr	May	Jun	Jul	Aug	Sep	Oct	Nov	Dec	AVG
1993			0,84	0,77	0,85	0,55	0,52	0,51	0,53	0,72	0,90	0,80	0,70
1994	0,83	0,83	0,80	0,78	0,56	0,33	0,28	0,40	0,43	0,70	0,89	0,91	0,64
1995	0,98	0,94	0,95	0,77	0,61	0,38	0,39	0,43	0,55	0,71	0,86	0,91	0,71
1996	0,92	0,87	0,89	0,72	0,57	0,31	0,23	0,50	0,72	0,74	0,50	0,87	0,65
1997	0,86	0,75	0,67	0,70	0,43	0,42	0,32	0,40	0,44	0,67	0,70	0,82	0,60
1998	0,79	0,71	0,75	0,53	0,76	0,48	0,24	0,13	0,35	0,46	0,78	0,78	0,56
1999	0,74	0,72	0,64	0,45	0,47	0,35	0,17	0,28	0,34	0,68	0,82	0,71	0,53
2000	0,84	0,60	0,52	0,52	0,29	0,30	0,15	0,26	0,38	0,47	0,52	0,74	0,47
2001	0,72	0,75	0,61	0,62	0,42	0,26	0,14	0,21	0,33	0,45	0,70	0,89	0,51
2002				0,52	0,26	0,32	0,20	0,32	0,37	0,54	0,59	0,77	0,43
2003	0,78	0,80	0,64	0,51	0,19	0,12	0,35	0,22	0,48	0,63	0,75	0,77	0,52
2004	0,90	0,89	0,71	0,51	0,48	0,36	0,20	0,41	0,29	0,55	0,67	0,71	0,56
2005	0,79	0,84	0,75	0,54	0,46	0,34	0,27	0,24	0,45	0,52	0,76	0,81	0,56
2006	0,90	0,80	0,72	0,57	0,48	0,31	0,34	0,36	0,81	0,84	0,75	0,72	0,63
2007	0,79	0,82	0,69	0,49	0,35	0,29	0,12	0,28	0,37	0,52	0,67	0,83	0,52
2008	0,75	0,69	0,57	0,65	0,34	0,26	0,29	0,21	0,57	0,42	0,56	0,73	0,50
2009	0,72	0,82	0,71	0,31	0,36	0,21	0,35	0,27			0,62	0,84	0,52
2010	0,91	0,85	0,69	0,44	0,28	0,48	0,37	0,26	0,38	0,66	0,45	0,70	0,54
2011	0,83	0,85	0,69	0,67	0,48	0,34	0,23	0,22	0,26	0,63	0,70	0,75	0,56
2012	0,93	0,87	0,71	0,47	0,58	0,19	0,21	0,35	0,24	0,45	0,69	0,78	0,54
AVG	0,83	0,80	0,71	0,58	0,46	0,33	0,27	0,31	0,44	0,60	0,69	0,79	0,56

Table 3. Statistical table of yearly average cloudiness

Year	1993	1994	1995	1996	1997	1998	1999	2000	2001	2002
Minimum	0,003	0,003	0,003	0,003	0,003	0,003	0,003	0,003	0,003	0,004
Maximum	1,000	1,000	1,000	1,000	1,000	1,000	1,000	1,000	1,000	1,000
Mean	0,697	0,636	0,701	0,652	0,592	0,555	0,526	0,463	0,486	0,429
Std. Dev.	0,063	0,053	0,052	0,058	0,059	0,059	0,060	0,061	0,058	0,064
Year	2003	2004	2005	2006	2007	2008	2009	2010	2011	2012
Minimum	0,003	0,003	0,003	0,003	0,003	0,003	0,003	0,003	0,003	0,375
Maximum	0,850	0,907	0,916	0,974	0,851	0,827	0,862	0,838	0,869	0,962
Mean	0,511	0,538	0,557	0,618	0,509	0,497	0,528	0,536	0,547	0,522
Std. Dev.	0,049	0,054	0,053	0,072	0,059	0,060	0,052	0,040	0,060	0,048

The highlighted values (in red) in table 2 and 3 are indication of either maximum or minimum values.

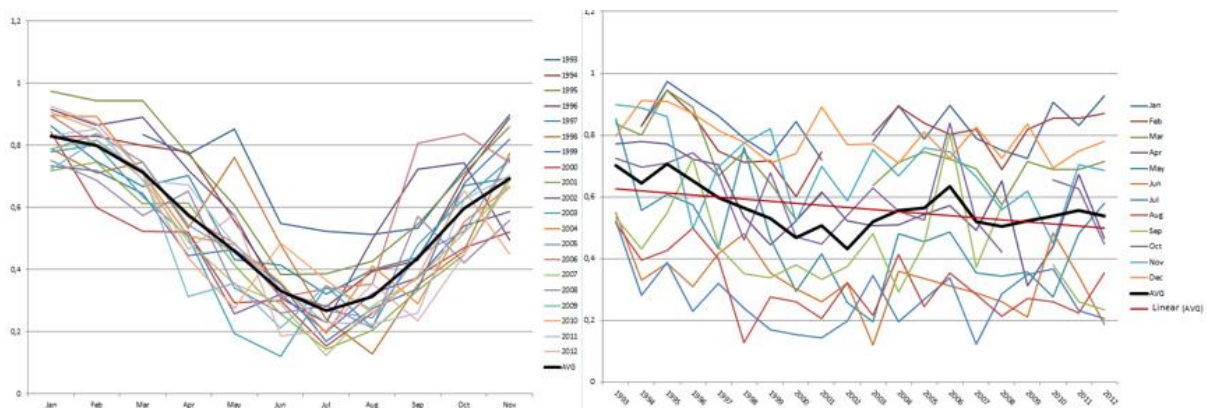


Figure 4. 20 year's average monthly cloudiness (%) of each month and yearly average cloudiness for 20 years (1993-2012).

Figure 4 shows the average monthly cloud cover over the Black Sea. As expected, cloud density is high during the winter and low during the summer. The main results of table 2 and Figure 4 are 1993 from May to August is quite off the average. In general Black Sea is 56% is cloudy. From statistical table highlighted in red June 2003 and January 1995, are 0,12% and 98% was cloudy with minimum and maximum respectively. Figure 4 showing 20 years average (thick black line) with linear trend line (thick red line) which shows decrease in the amount of cloud cover over the Black Sea.

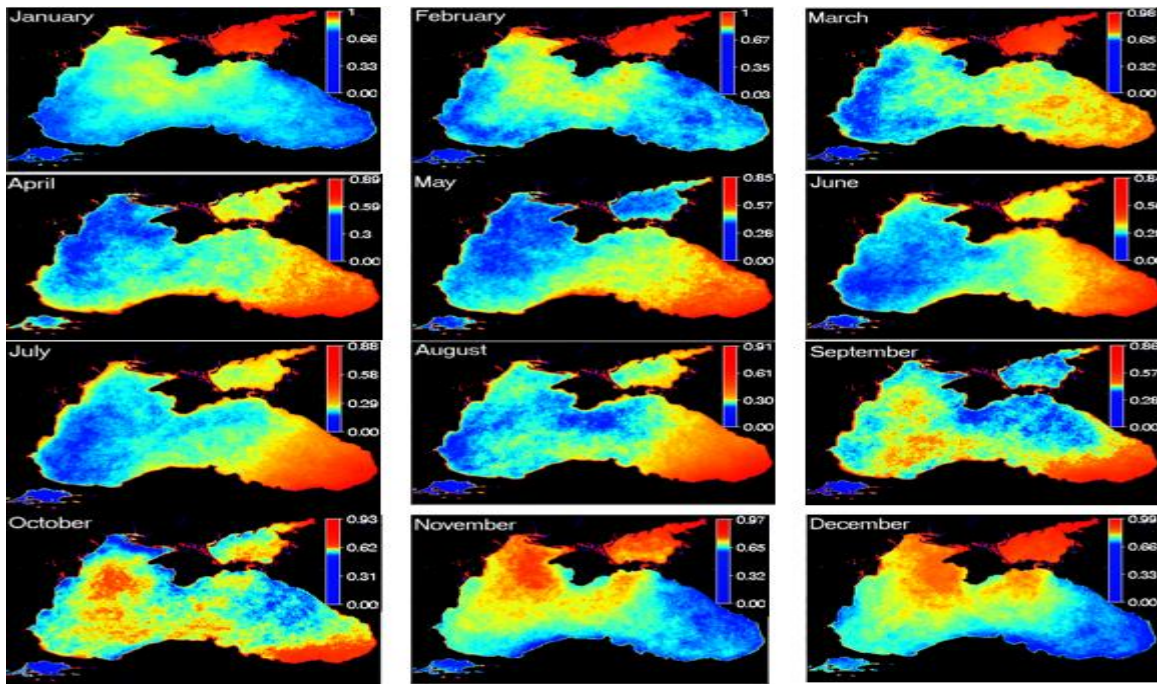


Figure 6. 20 year's average cloudiness (%) of each month (1993-2012).

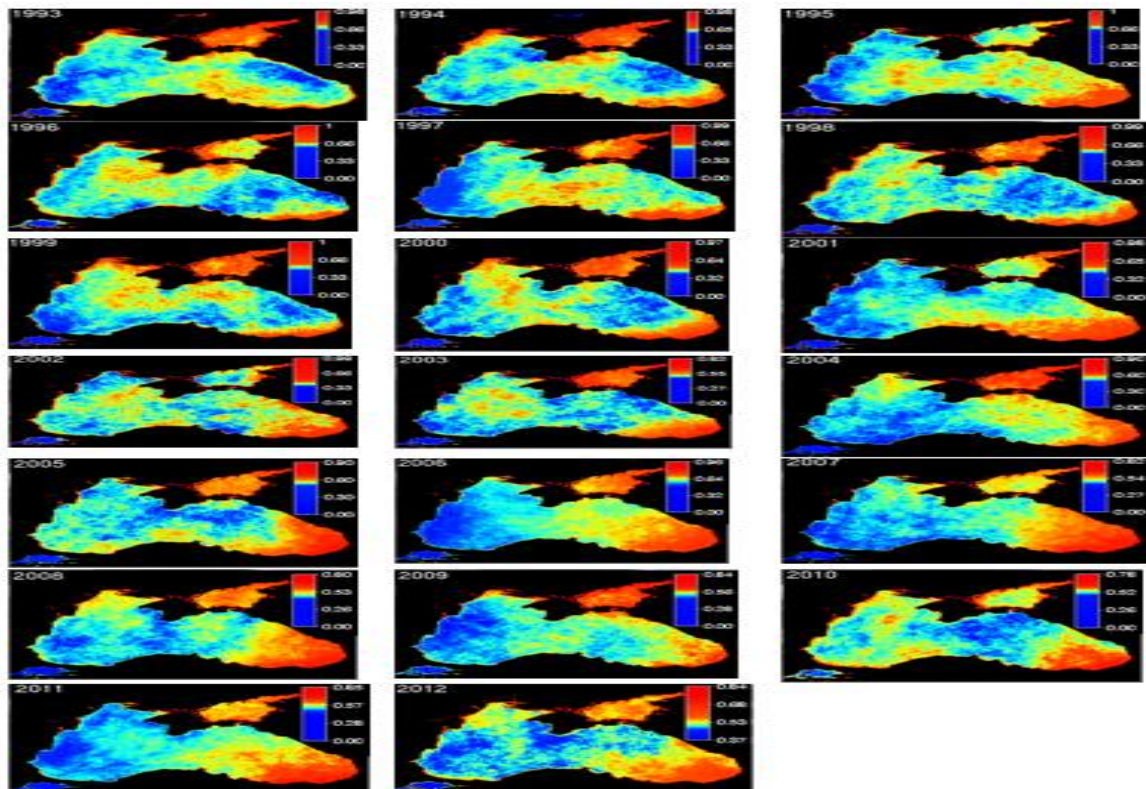


Figure 7. Yearly average cloud pattern (%) for each year (1993-2012).

The climatic conditions of the Black Sea and its surroundings are under the effect of general circulation of atmosphere and physical geography (especially high mountains surrounding eastern Black Sea region act like a wall). A large part of the region, especially in the north polar introduced under the influence of the air mass. However, these air masses, they come up to the main features of the source field is undergoing some changes. Most of the time the Black Sea undergoes to polar air masses from the north which causes high cloud cover particularly eastern Black Sea. Prevailing wind direction, depending on the pressure conditions and anticyclone cyclonic conditions, Rossby waves in the upper levels of the atmosphere, the North Atlantic and Arctic oscillations, the Black Sea and around important role to play.

3.2. Sea surface temperature

A total of 206 monthly composite SST images were downloaded from aforementioned DLR web site to process SST of the BS. The result presented on figure 8, 9.

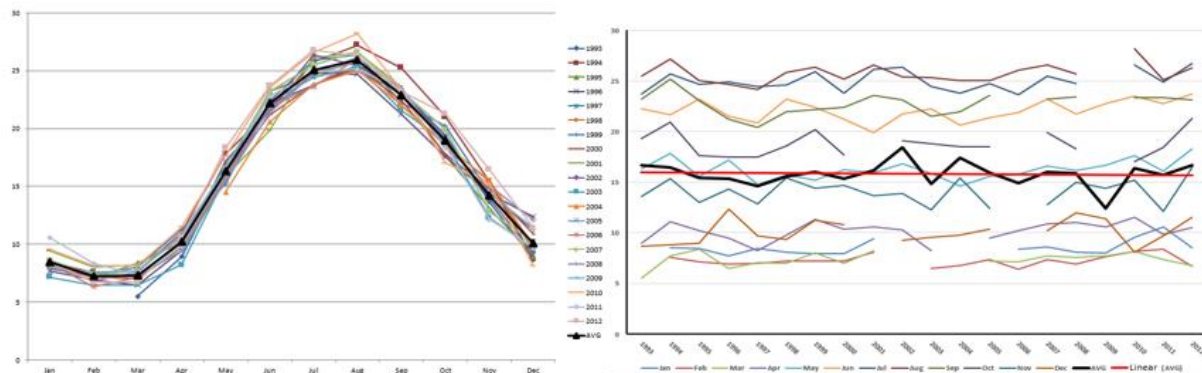


Figure 8. Seasonal variation of SST for 20 years in °C (Celsius) and yearly average SST for 20 years in °C (Celsius).

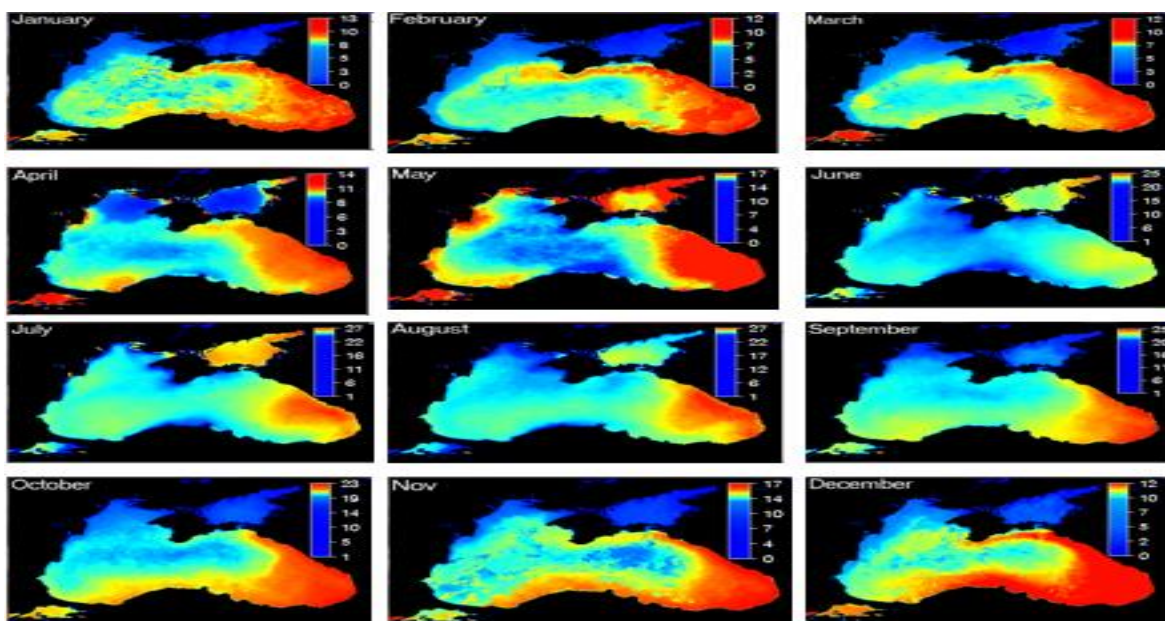


Figure 9. 20 year's average SST pattern for each °C (Celsius).

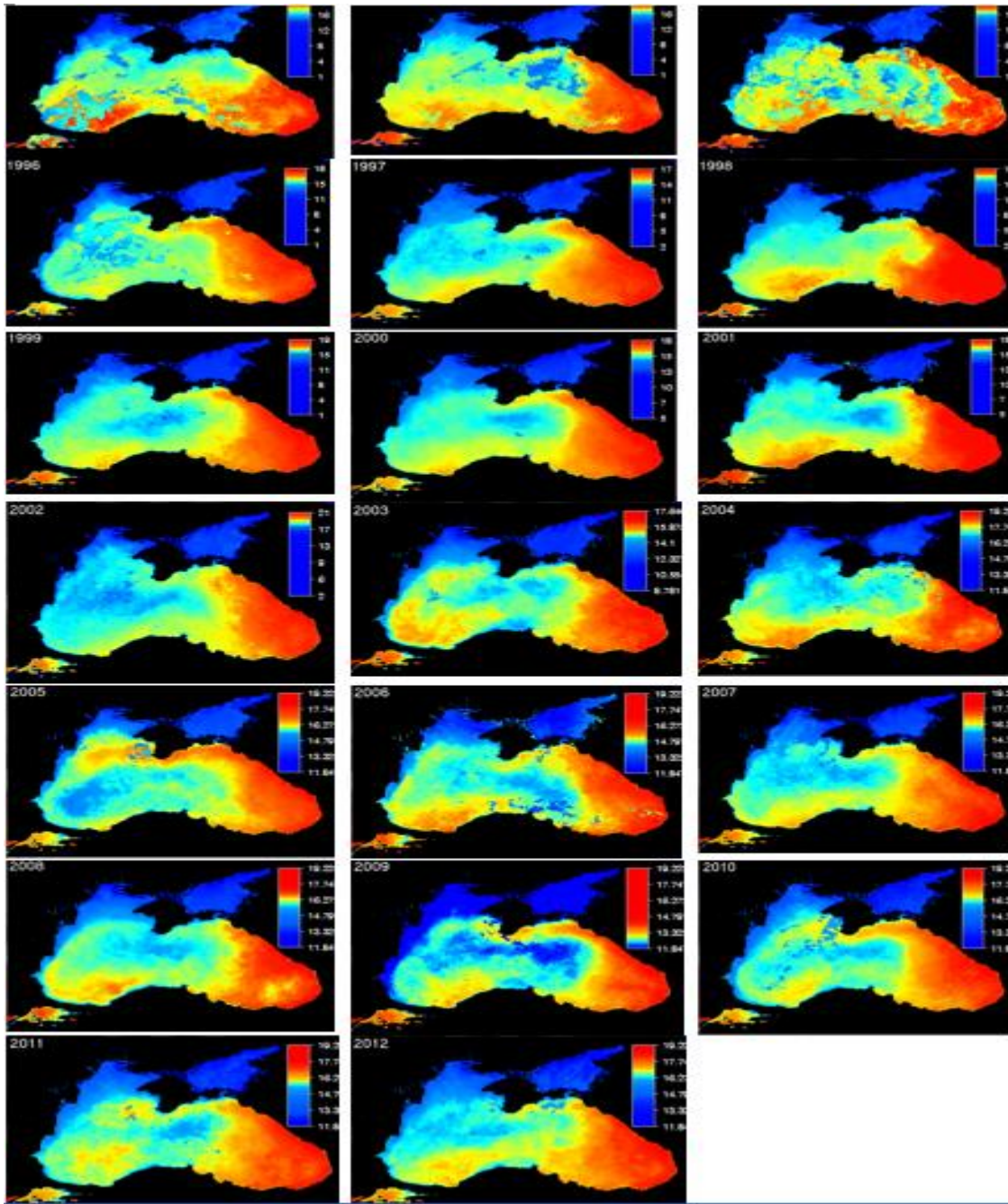


Figure 10. Yearly average SST pattern for 20 years in °C (Celsius).

Figure 9-10 are showing monthly and yearly average of SST pattern for the BS over 20 years. From November to February where polar air masses effective low cloud cover observed at eastern part of the BS this causes eastern part of the sea to be exposed to solar heating therefore an increase in SST.

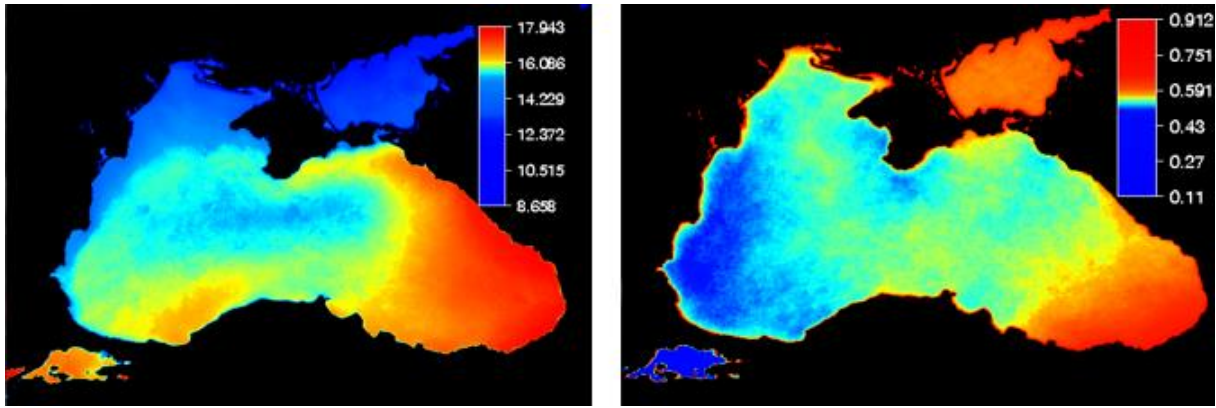


Figure 11. 20 year's average SST pattern °C (Celsius) and average cloud density pattern (%) respectively.

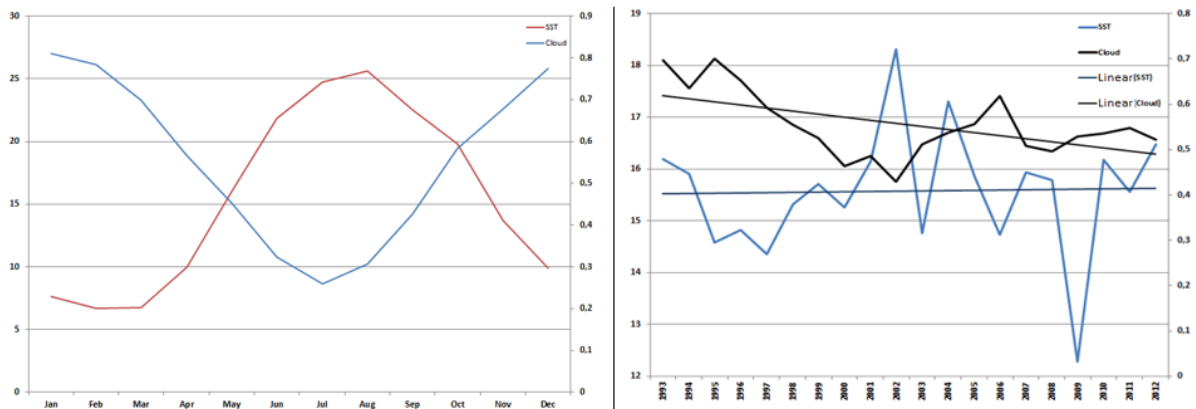


Figure 12. 20 year's average SST (°C) along with cloud density (%) and general trend of both for 20 years (1993-2012).

Figure 12 shows SST along with cloud cover, a lag between SST and cloud cover is due to thermal conductivity of water body. Trendline also shows a decrease on cloud cover accordingly a slight increase on SST with respect to each other.

4. Conclusion

In general, the possibility of compositing a 100% cloud free image of the Black Sea for a single day is impossible. This information may be used by people wishing to employ optical remote sensing with any kind of satellite since they may estimate the likelihood of there being cloud. Although in some cases quick looks are available, they may not give all the detail. This information would be factor when planning a remote sensing campaign, as it may save time and money. The potential availability may be found from Fig. 7 and 5.

Cloud density is high during the winter and low during the summer. The main results of table 2 and Fig.4 are from May to August 1993 and May to June 2003 are quite off the average. In general Black Sea is 56% is cloudy. From statistical table highlighted in red June 2003 and January 1995, are 0,12% and 98% was cloudy with minimum and maximum respectively. Linear trend line (thick red line) which shows decrease in the amount of cloud cover over the Black Sea. The climatic conditions of the Black Sea and its surroundings are under the effect of general circulation of atmosphere and physical geography. A large part of the region, especially in the north polar introduced under the influence of the air mass. However, these air masses, they come up to the main features of the source field is undergoing some changes. Most of the time the Black Sea undergoes to polar air masses from the north which causes high cloud cover particularly eastern Black Sea. Prevailing wind direction, depending on the pressure conditions and anticyclone cyclonic conditions, Rossby waves in the upper levels of the atmosphere, the North Atlantic and Arctic oscillations, the Black Sea and around important role to play

Monthly and yearly average of SST pattern for the BS over 20 years. From November to February where polar air masses effective low cloud cover observed at eastern part of the BS this causes eastern part of the sea to be exposed to solar heating therefore an increase in SST. Despite of low average cloud rate at the western side SST is lower due to geographic setting and cold water input from the rivers nearby. The results are also coherent with the Landscape formation of the Black Sea.

References

- [1] Ali, A., Quadir, D. A., & Huh, O. K. (1989). Studies of river flood hydrology in Bangladesh with AVHRR data. *International Journal of Remote Sensing*, 10, 1873-1891.
- [2] Atalay, İ. (2011). Türkiye iklim haritası. Ankara: İnkılap.
- [3] Barale., V., Gower, J. F. R., & Alberotanza, L. (2010). *Oceanography from Space*. Springer Dordrecht Heidelberg London New York: Springer.
- [4] Bromwich, D. H., Carrasco, J. F., & Stearns, C. R. (1992). Satellite-Observations of Katabatic-Wind Propagation for Great Distances across the Ross Ice Shelf. *Monthly Weather Review*, 120(9), 1940-1949. doi: Doi 10.1175/1520-0493(1992)120<1940:Sookwp>2.0.Co;2
- [5] Brown, R., Wooster, M., Blake, B., Sear, C., Huntchinson, P., & Stromme, T. (1993, 29 June-2 July). Use of real time AVHRR (Advanced High Resolution Radiometer) imagery to assess fishery conditions off Namibia. *Proceedings of 6th AVHRR Data Users' Meeting*, 385-392.
- [6] Byrd, G. (1998). *Lake Effect Snow*. University Corporation for Atmospheric Research.
- [7] Carey, R. M., & Pritchard, J. (1989). Flooding in Bangladesh. *Photogrammetric Engineering Remote Sensing*, 55(974).
- [8] Collins, M. J. (1989). Synoptic Ice Motion from Avhrr Imagery - Automated Measurements Versus Wind-Driven Theory. *Remote Sensing of Environment*, 29(1), 79-85. doi: Doi 10.1016/0034-4257(89)90080-1
- [9] Corel. (2012). Retrieved 2012, from <http://www.corel.com/en-eu/>
- [10] Cracknell, A. P. (1997). *Advanced Very High Resolution Radiometer*: Taylor & Francis.

- [11] Cracknell, A. P., & Huang, W. G. (1988). Surface Currents Off the West-Coast of Ireland Studied from Satellite Images. *International Journal of Remote Sensing*, 9(3), 439-446.
- [12] DLR. (2013). EOC Earth Observation Data - DLR. Retrieved 4 September, 2010, from <http://eoweb.dlr.de:8080/index.html>
- [13] Domain, F., & Citeau, J. (1980, 18-19 December 1979). Sea surface temperatures studied by Meteosat data along the coast of Senegal and Mauritania. Coastal and marine application of remote sensing.
- [14] ERMapper. from <http://www.hexagongeospatial.com/products/remote-sensing/erdas-imagine/overview>
- [15] Erol, O. (1993). Genel Klimatoloji. Ankara: Gazi Büro.
- [16] Foerster, J. W. (1993). Northeast North Pacific-Ocean - Surface Current Pattern Shifts during the Spring. *Remote Sensing of Environment*, 43(2), 149-159. doi: Doi 10.1016/0034-4257(93)90004-H
- [17] Geerts, B. (1998). Lake Effect Snow. from http://www-das.uwoyo.edu/~geerts/cwx/notes/chap10/lake_effect_snow.html
- [18] Geospatial, H. (2014). ERMapper. Retrieved 10 September, 2014, from <http://www.hexagongeospatial.com/>
- [19] Ginzburg, A. I., Kostianoy, A. G., & Sheremet, N. A. (2004). Seasonal and interannual variability of the Black Sea surface temperature as revealed from satellite data (1982-2000). *Journal of Marine Systems*, 52(1-4), 33-50. doi: DOI 10.1016/j.jmarsys.2004.05.002
- [20] Glenn, S. M., Forristall, G. Z., Cornillon, P., & Milkowski, G. (1990). Observation of Gulf Stream Ring 83-E and their interpretation using feature models. *Journal of Geophysical Research*, 95, 13043-13063.
- [21] Huh, O. K., & Shim, T. (1987). Satellite observations of surface temperatures and flow patterns, Sea of Japan and East China Sea, late March 1979. *Remote Sensing of Environment*, 22, 379-393.
- [22] Inoue, J., Kawashima, M., Fujiyoshi, Y., & Wakatsuchi, M. (2005). Aircraft observations of air-mass modification over the Sea of Okhotsk during sea-ice growth. *Boundary-Layer Meteorology*, 117(1), 111-129. doi: DOI 10.1007/s10546-004-3407-y
- [23] Jönsson, L. (1989, September 5-8). Flow studies of the northern part of the Strait of Öresund by means of remote sensing, 229-234.
- [24] Kikuchi, T., Satow, K., Ohata, T., Yamanouchi, T., & Nishio, F. (1992). Wind and Temperature Regime in Mizuho Plateau, East Antarctica. *International Journal of Remote Sensing*, 13(1), 67-79.
- [25] Koçman, A. (1993). Türkiye İklimi. İzmir: Ege Üniversitesi Edebiyat Fakültesi Yayınları.
- [26] Library, U. G.-A. M. a. G. (2001). Socio-economic indicators for the countries of the Black Sea basin. Retrieved Accessd December 11, 2010., from <http://www.grida.no/graphicslib/tag/black-sea>

- [27] Lonseth, L., & Bern, T.-I. (1991, June 25-28). Operational use of AVHRR (Advanced High Resolution Radiometer) products to monitor the Norwegian coastal current. Proceedings of 5th AVHRR Data Users' Meeting, 313-319.
- [28] Maul, G. A. (1985). Introduction to Satellite Oceanography. Boston, MA.: Martinus Nijhoff Publishers.
- [29] McClimans, T. A. (1989). Activities at the Norwegian-Hydrotechnical-Laboratory. International Journal of Remote Sensing, 10(4-5), 617-623.
- [30] Moctezuma, M., Maitre, H., & Parmiggiani, F. (1993). Automatic tracking of ice floes on AVHRR images sequences. Darmstadt-Eberstadt: EUMETSAT.
- [31] Murray, J. W., Jannasch, H. W., Honjo, S., Anderson, R. F., Reeburgh, W. S., Top, Z., . . . Izdar, E. (1989). Unexpected changes in the oxic/anoxic interface in the Black Sea. Nature, 338, 411 - 413. doi: 10.1038/338411a0
- [32] Nikitin, P. A. (1991). Satellite-based monitoring of sea ice. Darmstadt-Eberstadt: EUMETSAT.
- [33] Oguz, T., Latun, V. S., Latif, M. A., Vladimirov, V. V., Sur, H. I., Markov, A. A., . . . Unluata, U. (1993). Circulation in the Surface and Intermediate Layers of the Black-Sea. Deep-Sea Research Part I-Oceanographic Research Papers, 40(8), 1597-1612. doi: Doi 10.1016/0967-0637(93)90018-X
- [34] Özsoy, E., & Ünlüata, E. (1997). Oceanography of the Black Sea: a review of some recent results Earth-Science Reviews, 42, 231-272.
- [35] Paltridge, G. W., & Platt, C. M. (1976). Radiative Processes in Meteorology and Climatology. New York: Elsevier.
- [36] Prata, A. J., & Wells, J. B. (1990). A Satellite Sensor Image of the Leeuwin Current, Western-Australia. International Journal of Remote Sensing, 11(1), 173-180.
- [37] Sheng, Y., Xiao, Q., & Chen, W. (1993). Method of applying AVHRR data to monitor flood disaster. Darmstadt-Eberstadt: EUMETSAT.
- [38] Sheres, D., & Kenyon, K. E. (1990). An eddy, coastal jets and incoming swell all interacting near Pt Conception, California. International Journal of Remote Sensing, 11, 5-25.
- [39] Simpson, J. H., & Pingree, R. D. (1978). Shallow sea fronts produced by tidal string. In M. J. a. E. In Bowman, W.E. (eds) (Ed.), (Vol. 29). New York: Springer-Verlag.
- [40] Simpson, J. J., & Keller, R. H. (1995). An improved fuzzy logic segmentation of sea ice, clouds, and ocean in remotely sensed Arctic imagery. Remote Sensing of Environment, 54(3), 290-312. doi: Doi 10.1016/0034-4257(95)00175-1
- [41] Sousa, F. M., & Fiuza, A. (1989). Recurrence of upwelling filaments off northern Portugal as revealed by satellite imagery. Darmstadt-Eberstadt: EUMETSAT.
- [42] Studies, U. o. D. C. o. M. (2003). Surface Area—Black Sea Geography. Retrieved 2015, from <https://www.ceoe.udel.edu/blacksea/geography/index.html>

- [43] Swithinbank, C. (1973). Higher Resolution Satellite Pictures. *Polar Rec*, 16(104), 739-751.
- [44] Tanaka, S., Sugimura, T., Nishimura, T., Ninomiya, Y., & Hatakeyama, Y. (1982). Compilation of the Kuroshio Current vector map from NOAA-6/AVHRR (Advanced High Resolution Radiometer) data and consideration of oceanic eddies and the short period fluctuation of the Kuroshio. *Journal of Remote Sensing Society of Japan*, 2, 11-30.
- [45] Vastano, A. C., Borders, S., & Wittenberg, R. (1985). Sea surface flow estimation with infrared and visible imagery. *Journal of Atmospheric and Oceanic Technology*, 2, 401-403.
- [46] Vastano, A. C., & Borders, S. E. (1984). Sea-Surface Motion over an Anticyclonic Eddy on the Oyashio Front. *Remote Sensing of Environment*, 16(1), 87-90. doi: Doi 10.1016/0034-4257(84)90029-4
- [47] Vaughan, R. A., & Downey, I. D. (1988). Circulation patterns in AVHRR (Advanced High Resolution Radiometer) imagery. *International Journal of Remote Sensing*, 9, 597-600.
- [48] Viehoff, T. (1989). Mesoscale Variability of Sea-Surface Temperature in the North-Atlantic. *International Journal of Remote Sensing*, 10(4-5), 771-785.
- [49] Viola, A., & Böhm, E. (1991). Satellite- and air-derived sea surface temperature measurement during TEMPO. Darmstadt-Eberstadt: EUMETSAT.
- [50] Zheng, Q., Klemas, V., & Huang, N. E. (1984). Dynamics of the Slope Water Off New-England and Its Influence on the Gulf-Stream as Inferred from Satellite Ir Data. *Remote Sensing of Environment*, 15(2), 135-153. doi: Doi 10.1016/0034-4257(84)90042-7.